Role of the van Hove singularity in the quantum criticality of the Hubbard model

K.-S. Chen,[1] S. Pathak,[1] S.-X. Yang,[1] S.-Q. Su,[2] D. Galanakis,[3] K. Mikelsons,[4] M. Jarrell,[1] and J. Moreno[1]
[1]*Department of Physics and Astronomy, Louisiana State University, Baton Rouge, Louisiana 70803, USA*
[2]*Oak Ridge National Laboratory, Oak Ridge, Tennessee 37831, USA*
[3]*Nanyang Technological University, Singapore 639798*
[4]*Department of Physics, Georgetown University, Washington, DC 20057, USA*
(Received 6 May 2011; revised manuscript received 21 October 2011; published 12 December 2011)

A quantum critical point is found in the phase diagram of the two-dimensional Hubbard model [Vidhyadhiraja *et al.*, Phys. Rev. Lett. **102**, 206407 (2009)]. It is due to the vanishing of the critical temperature associated with a phase-separation transition, and it separates the non-Fermi-liquid region from the Fermi liquid. Near the quantum critical point, the pairing is enhanced since the real part of the bare d-wave pairing susceptibility exhibits an algebraic divergence with decreasing temperature, replacing the logarithmic divergence found in a Fermi liquid [Yang *et al.*, Phys. Rev. Lett. **106**, 047004 (2011)]. In this paper, we explore the single-particle and transport properties near the quantum critical point using high-quality estimates of the self-energy obtained by *direct* analytic continuation of the self-energy from the continuous-time quantum Monte Carlo method. We focus mainly on a van Hove singularity coming from the relatively flat dispersion that crosses the Fermi level near the quantum critical filling. The flat part of the dispersion orthogonal to the antinodal direction remains pinned near the Fermi level for a range of doping that increases when we include a negative next-near-neighbor hopping t' in the model. For comparison, we calculate the bare d-wave pairing susceptibility for noninteracting models with the usual two-dimensional tight-binding dispersion and a hypothetical quartic dispersion. We find that neither model yields a van Hove singularity that completely describes the critical algebraic behavior of the bare d-wave pairing susceptibility found in the numerical data. The resistivity, thermal conductivity, thermopower, and the Wiedemann-Franz law are examined in the Fermi liquid, marginal Fermi liquid, and pseudogap doping regions. A negative next-near-neighbor hopping t' increases the doping region with marginal Fermi liquid character. Both T and negative t' are relevant variables for the quantum critical point, and both the transport and the displacement of the van Hove singularity with filling suggest that they are qualitatively similar in their effect.

DOI: 10.1103/PhysRevB.84.245107 PACS number(s): 74.40.Kb, 71.10.Fd, 74.72.−h, 71.10.Hf

I. INTRODUCTION

A plausible scenario for the high-temperature superconductivity in cuprates is based on the presence of a van Hove singularity corresponding to the saddle points in the single-particle energy dispersion.[1–4] These flat regions in the energy dispersion are directly observed in angle-resolved photoemission spectroscopy (ARPES) experiments on various cuprate compounds.[5–9] Recently, the van Hove singularity was also observed in the tunneling spectra of Bi-2201.[10] The presence of saddle points in the energy dispersion is also argued to lead to a superconducting instability in other correlated systems, e.g., graphene.[11] If the Fermi level is doped to coincide with the van Hove singularity, then the superconducting transition temperature can be greatly enhanced.

The van Hove scenario is also argued[12–14] to be responsible for the *marginal Fermi liquid* behavior[15] in which the lifetime broadening of the quasiparticles is of the order of its energy. Thus the van Hove scenario is argued to account for the linear-T resistivity,[13,14,16] T-independent thermopower,[13] the anomalous isotope effect,[14] etc.

There is numerical evidence for the presence of van Hove singularities in models of strongly correlated systems. The energy dispersion of one hole in an antiferromagnetic background has been considered in studies of the Hubbard model[17,18] and the t-J model.[19] These studies report the presence of extended saddle points. Assaad and Imada[17] found that the dispersion has a quartic dependence with momentum near the antinodal point $(\pi,0)$.

These examples of extended saddle points in various correlated superconducting systems, and their proximity to the Fermi level at the doping where the maximum transition temperature occurs, demonstrate that it is extremely important to understand the role played by these singularities. A plethora of scientific efforts have been devoted toward achieving this understanding.[20–41] At the simplest level, the role of the van Hove singularity may be interpreted within the BCS formalism. Here, the superconducting transition temperature, T_c, is determined by the condition $V\chi_0'(\omega=0)=1$, where χ_0' is the real part of the $q=0$ bare pairing susceptibility and V is the strength of the pairing interaction. In a BCS superconductor, $\chi_0'(\omega=0)$ displays a logarithmic divergence as $T\to 0$, yielding the BCS exponential form for T_c. The van Hove singularity enhances the divergence of $\chi_0'(\omega=0)$, yielding higher transition temperatures.

There is also strong evidence for a quantum critical point located beneath the superconducting dome in the cuprates, and in close proximity to the doping with the maximum T_c.[42,43] Above the quantum critical point, in a range of doping associated with marginal Fermi liquid behavior, the in-plane resistivity is known to vary linearly with T over a wide range of temperatures.[44–50] In the Fermi liquid region, the low-temperature resistivity varies as T^2. The resistivity increases as the doping decreases from the Fermi liquid into

 ©2011 American Physical Society

the pseudogap region. Moreover, the thermal conductivity κ,[51,52] the thermopower S,[53,54] and the tunneling conductance g[55] have been investigated near the quantum critical point of the cuprates. κ is observed to be nearly independent of temperature in the marginal Fermi liquid state[56] and depends on $1/T$ in the Fermi liquid region. This is consistent with the Wiedemann-Franz law,[57] $\kappa\rho \propto T$. Chakraborty *et al.*[53] suggested that the thermopower changes sign abruptly near the optimal doping in most of the cuprate materials, signaling a state with particle-hole symmetry. Also in the marginal Fermi liquid, the tunneling conductance $g(V) \sim g_0 + g_1|V|$, where g_0 and g_1 depend weakly on T and V.

A recent study[58] reported the presence of a quantum critical point in the two-dimensional Hubbard model, where the quasiparticle spectral weight becomes zero. This quantum critical point separates the non-Fermi-liquid pseudogap from the Fermi liquid region, and is surrounded by a superconducting dome (cf. the inset in Fig. 1). At finite temperatures, the Fermi liquid and pseudogap regions are separated by the marginal Fermi liquid. Interestingly, at the quantum critical point, the density of states is found to be nearly particle-hole symmetric at low frequencies with a sharp peak at $\omega = 0$. This filling is tantalizingly close to the optimal doping where the superconducting transition temperature T_c attains its maximum. The proximity of the superconducting dome to the quantum critical point was recently investigated by Yang *et al.*[59] Unlike the BCS case, they found that the bare d-wave pairing susceptibility $\chi'_{0d}(\omega = 0)$ diverges algebraically as $\frac{1}{\sqrt{T}}$ at the quantum critical point, thus leading to a strongly enhanced T_c. Using the Kramers-Krönig relation between the real part and the imaginary part of the susceptibility, $\chi'_{0d}(T) = \frac{1}{\pi}\int \frac{\chi''_{0d}(\omega)}{\omega} d\omega$, the algebraic divergence of $\chi'_{0d}(T)$ was found to come from a scaling behavior of the imaginary part $\chi''_{0d}(\omega)$. When $T^{3/2}\chi''_{0d}(\omega)/\omega$ is plotted against ω/T, the different temperature curves fall on top of each other when $\omega \geqslant T_s \equiv 4tT/J$, determining a scaling function $H(x)$ such that $T^{3/2}\chi''_{0d}(\omega)/\omega = H(\omega/T) \approx (\omega/T)^{-3/2}$ (see Fig. 1). The contribution from H to $\chi'(T) = \frac{T^{-3/2}}{\pi}\int H(\omega/T)d\omega \propto T^{-1/2}$, which will dominate at low T.

Since this enhanced behavior is expressed in the bare pairing bubble, dressed by the self-energy but with no vertex corrections, this discussion naturally raises the question of the role played by the van Hove singularity in the quantum criticality and its possible connection to the superconducting T_c. In this paper, we use the dynamical cluster quantum Monte Carlo method to explore the relationship between the quantum critical point and the van Hove singularity for high-temperature superconductivity in the Hubbard model. We obtain high-quality estimates of the real-frequency single-particle self-energy $\Sigma(\boldsymbol{K},\omega)$ at the cluster momenta $\boldsymbol{K}$ by direct analytic continuation of the Matsubara frequency self-energy $\Sigma(\boldsymbol{K},i\omega_n)$ using the maximum entropy method.[60,61] This direct method avoids the artifacts on the self-energy that come about by inverting the coarse-grained Dyson's equation.[60] In the model without next-near-neighbor hopping ($t' = 0$), we find that, as we dope the system across the quantum critical filling, a flat region in the dispersion crosses the Fermi level, accompanied by a sharp nearly symmetric peak in the density of states that also passes through the Fermi level. We find that the resistivity follows a linear-T dependence over a wide range of temperatures yet a narrow range of doping (see Fig. 14). We use these high-quality estimates of the self-energy to calculate the bare pairing susceptibility; we again find the collapse of the data found in Fig. 1. To understand the role played by the van Hove singularity in determining this critical behavior, we have calculated the pairing susceptibility in the d channel for two noninteracting models at half-filling—the standard quadratic dispersion and a hypothetical quartic dispersion. While the quartic dispersion can yield the observed algebraic divergence of $\chi'_{0d}(\omega = 0)$, neither dispersion produces the collapse of the data found in Fig. 1, suggesting that a van Hove singularity alone does not capture this phenomenon. For negative t', the resistivity follows a linear-T behavior over a wider range of doping, and the sharp peak in the density of states and the flat region of the dispersion linger near the Fermi level for the same wider range of doping. These results suggest that the doping region affected by quantum criticality at low temperature becomes larger when $t' < 0$. We also show that the zero-frequency imaginary part of the self-energy $\Sigma''(T,\omega = 0)$, the dominant contribution to the resistivity, has a wider range of linear-T behavior for $t' < 0$ than $t' = 0$. All this motivates us to speculate a phase diagram near the quantum critical point in the Discussion section.

This paper has been organized as follows. Section II briefly outlines the model and methods used in this study. Results are presented in Sec. III. Single-particle properties are discussed

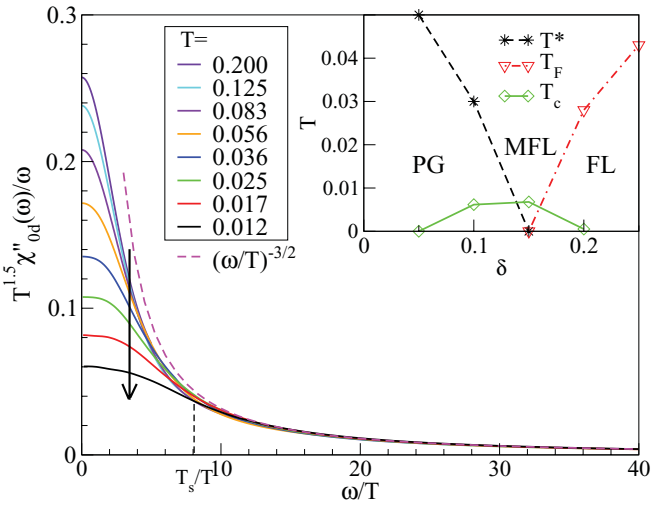

FIG. 1. (Color online) Frequency dependence of the imaginary part of the particle-particle d-wave susceptibility obtained from the dynamical cluster approximation for various temperatures at the critical filling $n = 0.85$ when $U = 6t$, $t' = 0$, and $4t = 1$. The arrow denotes the direction of decreasing temperature. All the curves fall on top of each other for frequencies greater than $T_s/T \approx 4t/J$. The inset shows the phase diagram for the same parameters (t, t', and U), including the Fermi liquid (FL), marginal Fermi liquid (MFL), and pseudogap (PG) regions. The lines indicate the d-wave transition temperature T_c (determined by extrapolation of data from $N_c = 8$-, 12-, and 16-site clusters), the pseudogap temperature T^*, and the Fermi liquid temperature T_F. (Taken from Yang *et al.*[59]) The quasiparticle fraction on the Fermi surface vanishes at the quantum critical point where $T^* = T_F = 0$, and remains zero in the pseudogap region.[58]

in Sec. III A, the pairing susceptibility calculation in Sec. III B, the effect of t' on the dispersion in Sec. III C, and transport results in Sec. III D. The broader implications of our results are discussed in Sec. IV and the paper is concluded in Sec. V.

II. FORMALISM

In this work, we look for direct evidence of the van Hove singularity and marginal Fermi liquid behavior in the spectra, electronic dispersion, and transport properties of the two-dimensional Hubbard model,

$$H = \sum_{\boldsymbol{k}\sigma} \epsilon^0_{\boldsymbol{k}} c^\dagger_{\boldsymbol{k}\sigma} c_{\boldsymbol{k}\sigma} + U \sum_i n_{i\uparrow} n_{i\downarrow}, \tag{1}$$

where $c^\dagger_{\boldsymbol{k}\sigma}$ ($c_{\boldsymbol{k}\sigma}$) is the creation (annihilation) operator for electrons with wave vector $\boldsymbol{k}$ and spin σ, $n_{i\sigma} = c^\dagger_{i\sigma} c_{i\sigma}$ is the number operator, and the bare dispersion is given by

$$\epsilon^0_{\boldsymbol{k}} = -2t(\cos k_x + \cos k_y) - 4t'(\cos k_x \cos k_y - 1), \tag{2}$$

with t and t' being the hopping amplitude between the nearest-neighbor and the next-near-neighbor sites, respectively, and U is the on-site Coulomb repulsion.

We employ the dynamical cluster approximation (DCA)[62,63] with a quantum Monte Carlo algorithm as the cluster solver. The DCA is a cluster mean-field theory that maps the original lattice onto a periodic cluster of size $N_c = L_c^2$ embedded in a self-consistently determined host. This many-to-one map is accomplished by dividing the lattice Brillouin zone into cells centered at momenta $\boldsymbol{K}$, and coarse graining the lattice Green's functions by summing over the momenta labeled with $\tilde{\mathbf{k}}$ within each cell,

$$\bar{G}(\boldsymbol{K},\omega) = \frac{N_c}{N} \sum_{\tilde{\mathbf{k}}} G(\boldsymbol{K}+\tilde{\mathbf{k}},\omega), \tag{3}$$

where $\bar{G}$ and G are the coarse-grained and lattice single-particle propagators, respectively. The coarse-grained Green's function defines the cluster problem. Spatial correlations up to a range L_c within the cluster are treated explicitly, while those at longer length scales are described at the mean-field level. However, the correlations in time, essential for quantum criticality, are treated explicitly for all cluster sizes. To solve the cluster problem, we use the continuous-time quantum Monte Carlo method,[64] which has no Trotter error,[65] and the Hirsch-Fye quantum Monte Carlo method[66,67] for the charge polarizability in Fig. 2. We employ the maximum entropy method[60] to calculate the real-frequency spectra.

A. Calculation of single-particle spectra

As in previous calculations of the single-particle spectra, we analytically continue the quantum Monte Carlo $\bar{G}(\boldsymbol{K},\tau)$ to obtain $\bar{G}(\boldsymbol{K},\omega)$, and then invert the coarse-graining Eq. (3) to obtain the self-energy $\Sigma(\boldsymbol{K},\omega)$. This last step can introduce spurious features in $\Sigma(\boldsymbol{K},\omega)$. As observed previously,[61] it is better to analytically continue the self-energy directly. However, the self-energy spectra do not share the normalization of $\int d\omega \bar{A}(\boldsymbol{K},\omega) = 1$, where $\bar{A}(\boldsymbol{K},\omega) = -\frac{1}{\pi}\bar{G}''(\boldsymbol{K},\omega)$. This normalization is a desirable feature since it allows us to treat the spectrum as a normalized probability distribution.

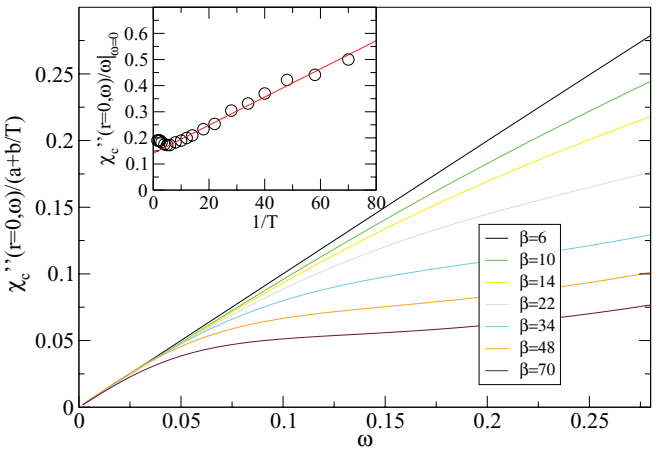

FIG. 2. (Color online) The local $\mathbf{r} = \mathbf{0}$ imaginary part of the dynamical charge polarizability divided by the initial slope at $\omega = 0$ for $n = 0.85$, $U = 6t$, $4t = 1$, $t' = 0$, and $N_c = 16$. It satisfies the marginal Fermi liquid form given by Eq. (8). Inset: the zero-frequency slope of $\chi_c''(\mathbf{r} = \mathbf{0},\omega)$ is roughly linear in inverse temperature, as expected. The line is a linear fit to the expression $a + b/T$.

Since the Hubbard self-energy $\Sigma(\boldsymbol{K},i\omega_n) = \Sigma_H + U^2\chi_{\sigma,\sigma}/i\omega_n + \cdots$, where $\chi_{\sigma,\sigma} = \langle n_\sigma n_\sigma\rangle - \langle n_\sigma\rangle^2 = n_\sigma(1-n_\sigma)$ is the local polarizability of a single spin species σ and $\Sigma(\boldsymbol{K},i\omega_n) - \Sigma_H = -\frac{1}{\pi}\int d\omega \frac{\Sigma''(\boldsymbol{K},\omega)}{i\omega_n - \omega}$, it is easy to see that the integral of $\Sigma(\boldsymbol{K},i\omega_n) - \Sigma_H$ is $U^2\chi_{\sigma,\sigma}$. Therefore, we will analytically continue

$$\frac{\Sigma(\boldsymbol{K},i\omega_n) - \Sigma_H}{U^2\chi_{\sigma,\sigma}} = \int d\omega \frac{\sigma(\boldsymbol{K},\omega)}{i\omega_n - \omega}, \tag{4}$$

where $\sigma(\boldsymbol{K},\omega) = -\frac{1}{\pi}\Sigma''(\boldsymbol{K},\omega)/U^2\chi_{\sigma,\sigma}$, $\int d\omega\, \sigma(\boldsymbol{K},\omega) = 1$, using $\chi_{\sigma,\sigma}$ calculated in the Monte Carlo process. After that, we obtain the lattice self-energy $\Sigma(\boldsymbol{k},\omega)$ by interpolating the cluster self-energy $\Sigma(\boldsymbol{k},\omega)$ to get the single-particle spectral function $A(\boldsymbol{k},\omega)$.

B. *d*-wave pairing susceptibility

We calculate the susceptibility in the d-wave channel to the pair field $\mathcal{V} = -f_d b_d^\dagger + \text{H.c.}$ for various models with a van Hove singularity at the Fermi level. Here $b_d^\dagger = \frac{1}{2}\sum_i (b^\dagger_{i+\hat{x}} - b^\dagger_{i+\hat{y}})$ is the singlet creation operator, where $b^\dagger_{i+\hat{\alpha}}$ creates a singlet at bond i-$(i+\hat{\alpha})$, $\alpha = x,y$, and f_d is a complex constant. The noninteracting d-wave pairing susceptibility χ_{0d} can be computed by calculating the susceptibility bubble

$$\chi_{0d}(T) = T \sum_{\boldsymbol{k},i\omega_n} g_d^2(\boldsymbol{k}) G^0(\boldsymbol{k},i\omega_n) G^0(-\boldsymbol{k},-i\omega_n), \tag{5}$$

where $g_d(\boldsymbol{k})$ is the d-wave form factor given by $g_d(\boldsymbol{k}) = \cos k_x - \cos k_y$. $G^0(\boldsymbol{k},i\omega_n)$ is the noninteracting Green function given by

$$G^0(\boldsymbol{k},i\omega_n) = \frac{1}{i\omega_n - \epsilon^0_{\boldsymbol{k}}}, \tag{6}$$

with $\epsilon_{\boldsymbol{k}}^0$ the bare band dispersion in Eq. (2). χ_{0d} can be evaluated using the standard Matsubara summation, which gives

$$\chi_{0d}(T) = \sum_{\boldsymbol{k}} g_d^2(\boldsymbol{k}) \left(\frac{1 - 2f_{\boldsymbol{k}}}{2\epsilon_{\boldsymbol{k}}^0} \right), \tag{7}$$

where $f_{\boldsymbol{k}}$ is the Fermi function.

C. Transport coefficients

To explain the anomalous transport properties of the marginal Fermi liquid, Varma *et al.*[15,68] postulated that for a wide range of wave vectors $\boldsymbol{q}$, excitations make a contribution to the absorptive spin and charge polarizabilities reflected by

$$\chi''(\boldsymbol{q},\omega) \propto \min(|\omega/T|,1)\,\mathrm{sgn}(\omega). \tag{8}$$

Electrons scattering from these excitations acquire a self-energy

$$\Sigma(\boldsymbol{k},\omega) \propto \omega \ln(x/\omega_c) - i\pi x/2, \tag{9}$$

where $x = \max(|\omega|,T)$, and ω_c is a cutoff. The marginal Fermi liquid ansatz has several consequences on experimentally relevant quantities, including transport anomalies, such as the linear-T electrical resistivity, the tunneling conductance $g(V) \sim g_0 + g_1|V|$, the photoemission, the nuclear relaxation rate $T_1^{-1} \sim aT + b$, the optical conductivity $\sigma(\omega)$, the Raman scattering, and the superconductive pairing. For the specific heat $C_v(T)$ and thermal conductivity $\kappa(T)$, Varma argued that the normal state's electronic contribution is hard to extract from the experimental data due to the large phonon contribution. The electronic thermal conductivity for the marginal Fermi liquid approximates to a constant because the Wiedemann-Franz law roughly holds.

To calculate the various Onsager transport coefficients, we use the Kubo formula:[69]

$$L_{\alpha\beta}^{ij} = \pi \int d\omega \left(-\frac{df}{d\omega} \right) \omega^{i+j-2} \mathcal{D}_{\alpha\beta}(\omega), \tag{10}$$

where f is the Fermi function and

$$\mathcal{D}_{\alpha\beta}(\omega) = \frac{1}{N} \sum_{\boldsymbol{k}} v^{\alpha}(\boldsymbol{k}) v^{\beta}(\boldsymbol{k}) A(\boldsymbol{k},\omega)^2, \tag{11}$$

where $v^{\alpha}(\boldsymbol{k})$ is the α-component of the electron group velocity and $A(\boldsymbol{k},\omega)$ is the single-particle spectral function. The different transport coefficients are given by combinations of L^{ij}. For example, in units where $e = 1$ and the chemical potential $\mu = 0$, the resistivity $\rho(T) = 1/L^{11}$, the thermopower $S = -L^{12}/TL^{11}$, the thermal conductivity $\kappa = \frac{1}{T}[L^{22} - (L^{12})^2/L^{11}]$, and the Peltier coefficient $\Pi = L^{21}/L^{11}$.

We note that a simpler estimate exists for the thermopower S. Here, we perform a Sommerfeld expansion of L^{12} at the Fermi level and get an alternative form:

$$S = -\frac{\pi^2}{3} T \left. \frac{\partial \log[\mathcal{D}_{\alpha\beta}(\omega)]}{\partial \omega} \right|_{\omega=0}. \tag{12}$$

If the electron group velocity is a constant, and the square of the single-particle spectra is approximated by $\delta(\omega - \epsilon_{\boldsymbol{k}})\tau_{\boldsymbol{k}}$, where $\tau_{\boldsymbol{k}}$ is the relaxation time, also assumed constant, the thermopower over temperature becomes just the derivative of the logarithm of the density of states at the Fermi level.[70]

III. RESULTS

A. Single-particle properties for $t' = 0$

We first explore the charge polarizability in the marginal Fermi liquid region at $n = 0.85$. The imaginary component of the local charge polarizability $\chi_c''(\boldsymbol{r} = 0,\omega)$ is plotted in Fig. 2. The main plot shows $\chi_c''(\boldsymbol{r} = 0,\omega)$ divided by its initial slope at zero frequency (determined in the inset), so that the curves coincide for low ω. At higher frequencies, the curves break from this linear rise at a frequency roughly proportional to the temperature. The inset shows that the zero-frequency slope, $\chi_c''(\boldsymbol{r} = 0,\omega)/\omega|_{\omega=0}$, is roughly linear in inverse temperature up to $T \approx 0.2$ or roughly $2J = 8t^2/U$. These features are consistent with the marginal Fermi liquid polarizability in Eq. (8). The spin polarization (not shown) does not display such an extended region of marginal Fermi liquid character. This result is consistent with marginal Fermi liquid behavior due to the proximity of a quantum critical point associated with phase separation.

Figure 3 shows the frequency dependence of the imaginary self-energy at the Fermi momenta along the antinodal ($X\Gamma$) and the nodal (ΓM) directions for three fillings: $n = 0.75$ (Fermi liquid), $n = 0.85$ (marginal Fermi liquid), and $n = 0.95$ (pseudogap). For the self-energy at $n = 0.75$, the quadratic dashed line (bottom right panel) provides a good fit to $\Sigma''(\boldsymbol{k}_F,\omega)$ for small ω, as expected from the Fermi liquid theory.[71] The marginal Fermi liquid self-energy has a form given by Eq. (9), which states that the imaginary self-energy is proportional to the negative temperature for small frequency and to the negative ω when the temperature is low. The marginal Fermi liquid self-energy in Fig. 3 (upper right panel) shows a linear behavior, but interestingly with *different* slopes for positive and negative ω. This is not consistent with Eq. (9), but this may be due to the presence of some short-range order. That is, Markiewicz *et al.*[72] calculated the self-energy

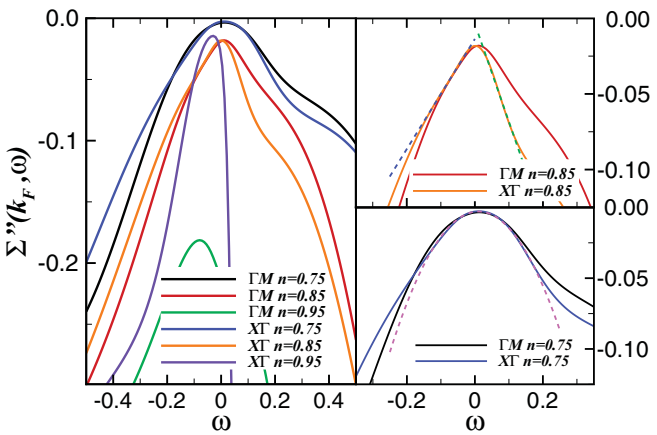

FIG. 3. (Color online) Frequency dependence of the imaginary part of the self-energy at the Fermi momentum, $\Sigma''(\boldsymbol{k}_F,\omega)$, along ΓM and $X\Gamma$ for $U = 6t, 4t = 1, t' = 0, N_c = 16$, and $\beta = 58$. Right panels show an enlarged view of the low-frequency region. Dashed lines fit the data linearly for $n = 0.85$ and quadratically for $n = 0.75$.

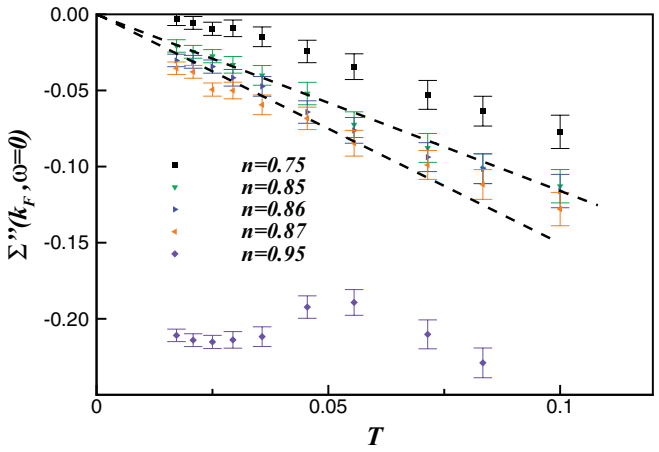

FIG. 4. (Color online) Temperature dependence of the imaginary part of the self-energy $\Sigma''(\boldsymbol{k}_F,\omega=0)$ at the Fermi energy and momenta, $U=6t$, $4t=1$, $t'=0$, and $N_c=16$. The linear dashed lines fit the self-energies for $n=0.85$ and 0.86 below $T=0.031$.

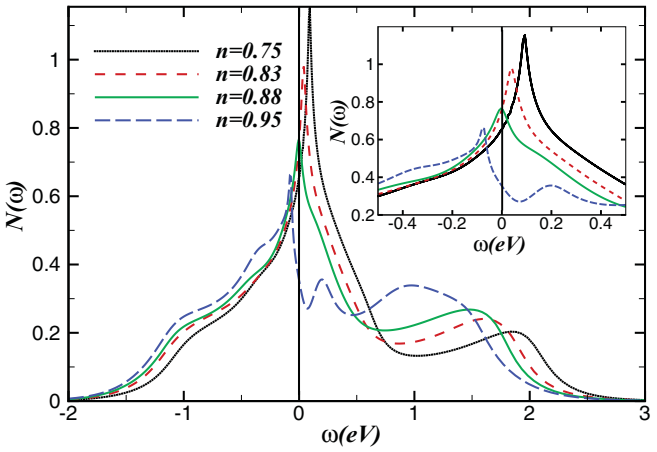

FIG. 5. (Color online) The single-particle density of states for $t'=0$, $U=6t$, $4t=1$, $N_c=16$, and $\beta=58$. The density of states shows low-energy particle-hole symmetry at the filling of $n=0.88$.

due to the random-phase approximation (RPA) magnetic polarizability for a single band model with dispersion obtained by a fitting to the tight-binding local-density approximation. They found that the self-energy has linear forms but with different slopes on positive and negative ω when the van Hove singularity is at the Fermi level and quadratic otherwise.

Figure 4 shows the temperature dependence of the self-energy when $\omega=0$ and $t'=0$. Again we find a result consistent with Eq. (9), $\Sigma''(\boldsymbol{k}_F,\omega\to 0)\propto -T$, around the marginal Fermi liquid filling for $n=0.85$ and 0.86. The dashed lines are linear fits. The error bars are estimated by changing the random seeds in the Monte Carlo calculation. However, they do not reflect the systematic error that comes from the bias toward the default model, which is the spectra from the next higher temperature in this case. This error is largest at low T, where the data are weak due to the minus sign problem.

The self-energy and dynamic charge polarizability near the critical filling $n_c=0.85$ are generally consistent with Varma's marginal Fermi liquid ansatz, as are the results found previously for the kinetic and potential energies, which vary with temperature like $T^2\ln(T)$[73] and the vanishing wave-function renormalization factor.[58] To understand the relationship of these results to the van Hove singularity, we will explore the density of states and the quasiparticle dispersion.

The density of states for several fillings is shown in Fig. 5. Since we have highly enhanced the quality of the self-energy by *direct* analytic continuation of $\Sigma(K,i\omega_n)$, the density of states in Fig. 5 shows sharper features as compared to the results of Vidhyadhiraja *et al.*[58] As the doping decreases from the Fermi liquid to the pseudogap region, the peak of the density of states moves from positive to negative energy while its intensity is reduced. For $n=0.95$, a pseudogap begins to open and a peak begins to form at positive frequencies. The half-filled case ($n=1$, not shown) shows upper and lower Hubbard bands located at positive and negative frequencies, respectively. The density of states for filling 0.88, close to the critical filling of 0.85, shows low-frequency particle-hole symmetry.

Figure 6 shows the dispersion obtained from the peaks of the spectral function $A(\boldsymbol{k},\omega)$ for four fillings: $n=0.85, 0.87, 0.88$, and 0.95, along the antinodal direction and around the Fermi vector $\boldsymbol{k}_F$. In order to define $\boldsymbol{k}_F$, we look for the maximum value of the zero-frequency spectral function $A(\boldsymbol{k},\omega=0)$. In the Fermi liquid and marginal Fermi liquid regions, this definition is roughly equivalent to the Luttinger surface defined where $G'(\boldsymbol{k},\omega=0)$ changes sign. The two definitions yield different results for the pseudogap region, especially when $t'<0$, which enhances the pseudogap. However, this difference is not large enough to qualitatively change our results or to change any of our conclusions. Therefore, for simplicity, we only show results using the first definition of $\boldsymbol{k}_F$. For a particular filling, the left panel shows the dispersion along the k_x direction ($k_y=0$), while the right panel shows the dispersion along k_y ($k_x=k_{Fx}$). A common identifiable feature for all fillings is the presence of a flat region in the dispersion. This flat region is responsible for the van Hove singularity in the density of states. The van Hove singularity passes through the Fermi level at a filling of $n\approx 0.88$, which is near the quantum critical filling, $n\approx 0.85$, where the quasiparticle weight Z goes to zero.[58] At this filling, the topology of the Fermi surface also changes from holelike [closed around the point $\boldsymbol{k}=(\pi,\pi)$] to electronlike [closed around $\boldsymbol{k}=(0,0)$] with increasing filling (not shown), as seen in experiments.[74] The dispersion along the k_y direction remains pinned near the Fermi level for a range of doping near the center of the superconducting dome, while the dispersion along the k_x direction passes continuously through the Fermi level. This anisotropic motion of the flat dispersion is consistent with a van Hove peak that moves continuously through the Fermi level, as shown in Fig. 5, and would correspond to a flat region at the Fermi level that is most isotropic at the crossing and shrinks to narrow pencil-like regions for fillings above and below the crossing.

The dispersion along the antinodal direction as a function of k_x for various fillings is displayed in Fig. 7. Interestingly, a quadratic form fits well to the data for all fillings. Next, we investigate whether such a dispersion can capture the critical algebraic divergence of the pairing susceptibility.

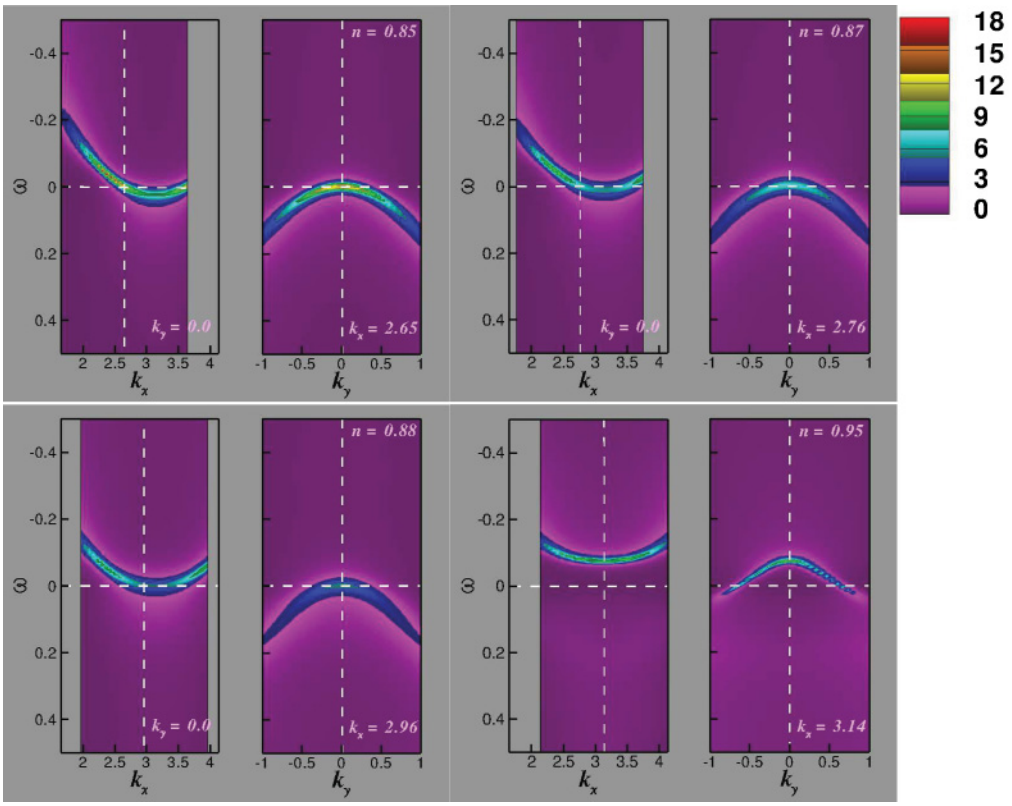

FIG. 6. (Color online) Energy dispersion obtained from the peaks of the spectral function $A(\boldsymbol{k},\omega)$ for various fillings around the Fermi vector $\boldsymbol{k}_F$ along the antinodal direction for $t' = 0$, $U = 6t$, $4t = 1$, $N_c = 16$, and $\beta = 58$. By fixing $k_y = 0$, we explore the dispersion along the k_x direction, and for $k_x = k_{Fx}$ the dispersion along the k_y direction is plotted. Notice that the energy axes are inverted so that positive energies are plotted down. The dispersion along the k_y direction remains pinned near the Fermi level for a range of doping near the center of the superconducting dome (cf. the inset of Fig. 1).

B. Pairing susceptibility

The density of states and the dispersion show clear evidence for a van Hove singularity that crosses the Fermi level near the critical filling. In order to see whether the van Hove singularity alone is sufficient to explain the enhanced bare pairing bubble, we calculate the pairing susceptibility in the d-wave channel

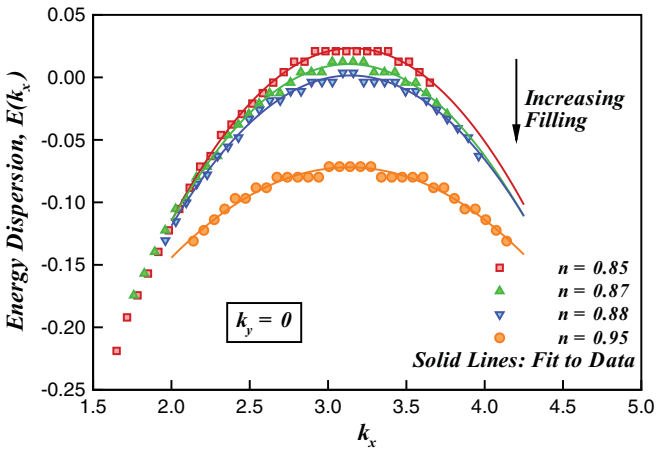

FIG. 7. (Color online) Single-particle dispersion around the Fermi energy taken along the antinodal direction ($k_y = 0$). The data is from Fig. 6. The solid lines are fits to a quadratic dispersion.

for two simple models having a van Hove singularity at the Fermi level. We begin with the tight-binding model given by Eq. (2) at half-filling and $t' = 0$. The associated density of states has a logarithmic singularity at $\epsilon = 0$, $N(\epsilon) = \log|\epsilon|$. The temperature dependence of χ'_{0d} can be obtained by converting Eq. (7) to an integral over energy with a temperature T cutoff. It results in a $-(\log T)^2$ behavior. This is confirmed by explicit calculation of the sum in Eq. (7), as illustrated in Fig. 8. As shown in the inset, the imaginary part does not show scaling behavior as seen in Fig. 1.

We also consider the next higher order model allowed by the symmetry of the square lattice, a hypothetical model with a quartic dispersion,

$$\epsilon_{\boldsymbol{k}} = -\frac{4}{\pi^4}\left[(|k_x| - \pi)^4 - k_y^4\right]. \tag{13}$$

Such an extended form has been observed in experiments[6] and also confirmed by theoretical studies.[18] The low-energy density of states for the quartic dispersion becomes $N(\epsilon) \sim 1/\sqrt{|\epsilon|}$.[27] Following a similar logic to that used for the tight-binding dispersion, for a quartic dispersion we get $\chi'_{0d} \sim \frac{1}{\sqrt{T}}$.

Results for the explicit calculation [Eq. (7)] are shown in Fig. 9, and are consistent with the analytical arguments above. Though the temperature dependence of the real part of the bare susceptibility is found to be algebraic for this quartic dispersion, the inset reveals that the imaginary pairing

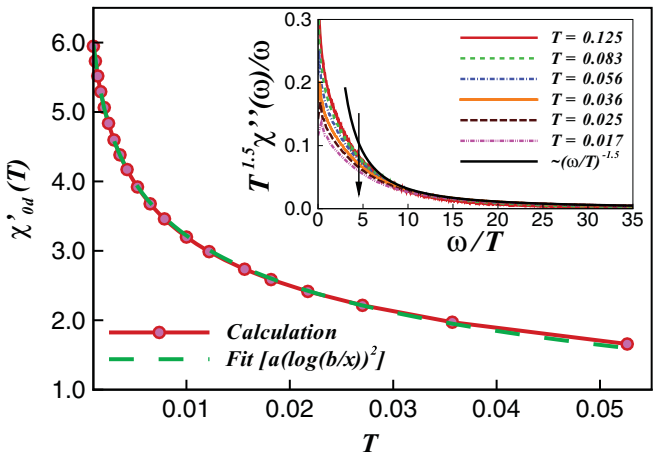

FIG. 8. (Color online) Temperature dependence of the real part of the particle-particle d-wave susceptibility at $\omega = 0$ for the two-dimensional tight-binding dispersion at half-filling. Note that χ'_{0d} diverges logarithmically as $T \to 0$. Inset: Frequency dependence of the imaginary part of the particle-particle d-wave susceptibility. Note that the curves corresponding to various temperatures do not scale at large frequency. The arrow denotes the direction of decreasing temperature.

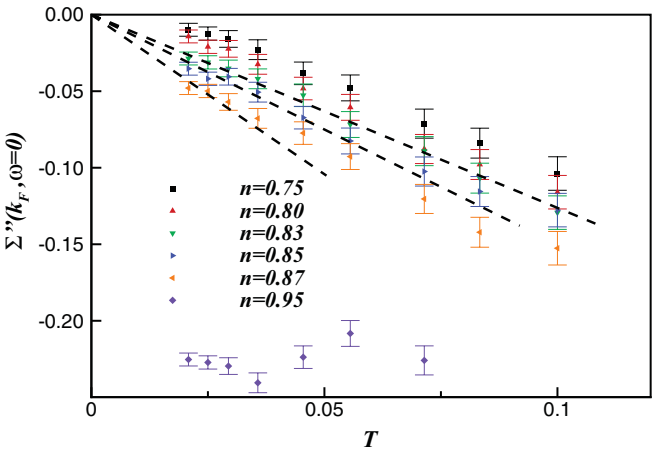

FIG. 10. (Color online) Temperature dependence of the imaginary part of the self-energy $\Sigma''(\boldsymbol{k}_F, \omega = 0)$ at the Fermi energy and momenta, $U = 6t$, $N_c = 16$, $4t = 1$, and $t'/t = -0.1$. The self-energy for fillings between $n = 0.83$ and 0.87 shows a linear-T behavior.

susceptibility does not exhibit the scaling found by Yang *et al.*[59] Thus, the simple noninteracting picture of the van Hove singularity at the Fermi level does not completely describe the true temperature and frequency dependence of the susceptibility.

C. Effect of negative t'

The single-band Hamiltonian used to model the hole-doped cuprates generally includes a negative next-near-neighbor hopping t'. For $t' = -0.1t$, the temperature dependence of the self-energy at the Fermi momenta and energy is shown in Fig. 10. We find that $\Sigma''(\boldsymbol{k}_F, \omega = 0)$ follows a linear behavior over a wider range of fillings, from $n = 0.83$ to 0.87.

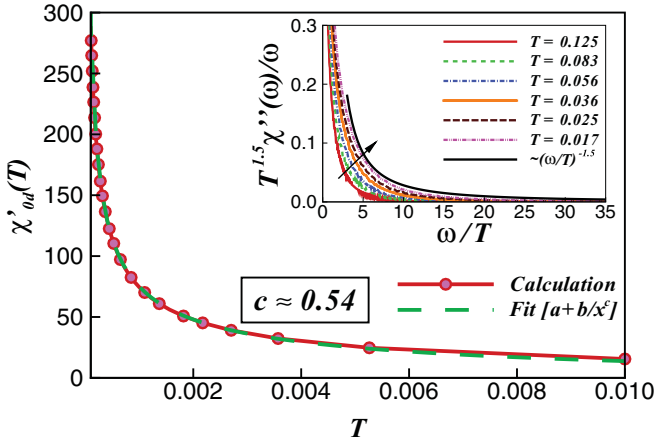

FIG. 9. (Color online) Temperature dependence of the real part of the particle-particle d-wave susceptibility at $\omega = 0$ for the quartic dispersion of Eq. (13) at half-filling. Note that χ'_{0d} diverges algebraically $\sim 1/\sqrt{T}$ as $T \to 0$. A fit to $a + b/x^c$ gives values of $a = -10.6$, $b = 1.98$, and $c = 0.54$. Inset: Frequency dependence of the imaginary part of the pairing d-wave susceptibility. Note that the curves corresponding to various temperatures do not scale well at large frequency. The arrow denotes the direction of decreasing temperature.

Figure 11 demonstrates that the inclusion of a negative t' also results in the pinning of the flat part of the k_y dispersion to the Fermi level. However, now the pinning is observed for a larger range of fillings, roughly 0.80 to 0.86. Thus both measurements, the temperature dependence of the self-energy and the pinning of the flat dispersion to the Fermi level, are consistent. If we take the viewpoint that the quantum critical point and the pinning of the dispersion along k_y to the Fermi level are concomitant aspects of quantum criticality, then a negative t' leads to a larger range of quantum critical fillings. We will also see the signature of this behavior in various transport properties discussed in Sec. III D.

Figure 12 shows the density of states for $t'/t = -0.1$ and various fillings as a function of ω. For a given filling, the inset of Fig. 12 shows that the peak in the density of states is slightly shifted to smaller frequencies when compared with the peak in the density of states for $t' = 0$. It displays particle-hole symmetry roughly at $n = 0.84$, not $n = 0.88$ as for $t' = 0$. Moreover, if we use $\Delta\omega_p/\Delta n$, where ω_p is the location of a peak in the density of states and n is the filling, to estimate the rate at which the peak crosses the Fermi level, we find that the peak of the density of states for $t' = 0$ crosses the Fermi level more quickly than the peak for negative t'. This can be seen in the inset of Fig. 12, where the filling dependence of the peak location has a steeper slope for $t' = 0$ than that for $t'/t = -0.1$ at the Fermi level. This confirms that negative t' leads to a *wider* range of fillings with a van Hove peak near the Fermi level. The fact that this range of fillings coincides with the region where marginal Fermi liquid behavior is seen in the self-energy suggests that the van Hove singularity and quantum criticality are related.

Another interesting point to be noted here is that, when compared to the $t' = 0$ result, the quasiparticle peaks become more incoherent for negative t'. This can be seen in the Matsubara

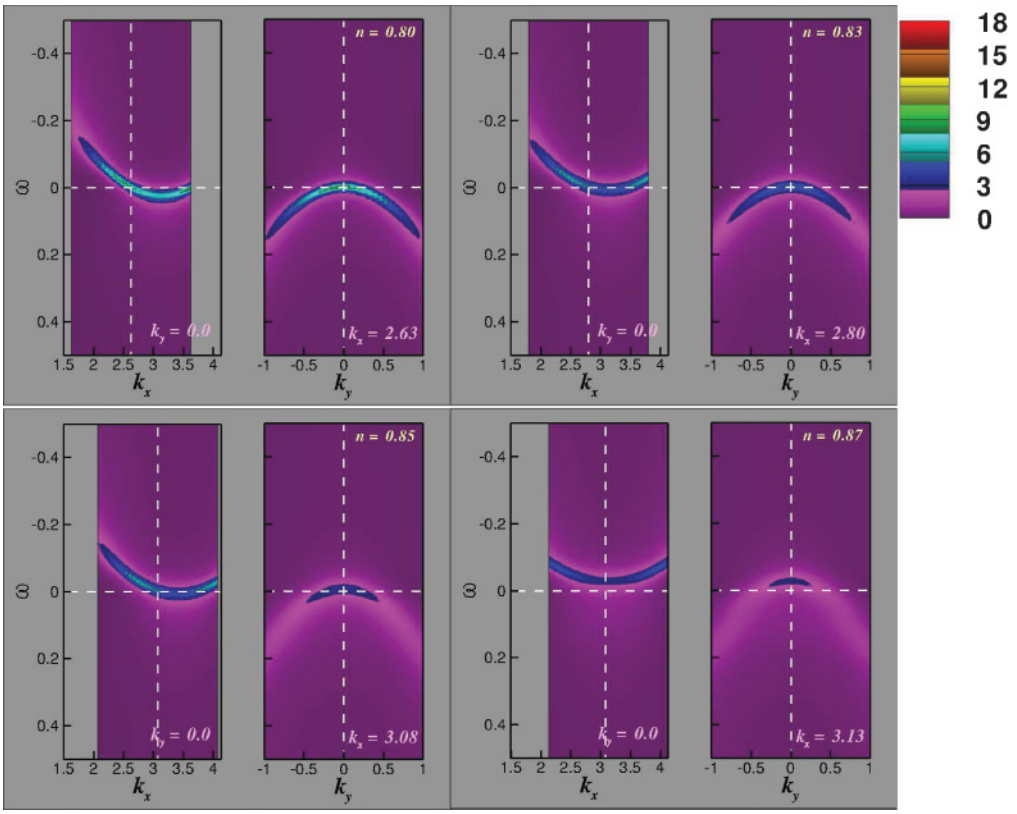

FIG. 11. (Color online) Energy dispersion obtained from the peaks of the spectral function $A(\boldsymbol{k},\omega)$ for various fillings around the Fermi vector $\boldsymbol{k}_F$ along the antinodal direction for $t'/t = -0.1$, $U = 6t$, $4t = 1$, $N_c = 16$, and $\beta = 48$. The dispersion along the k_y direction remains pinned near the Fermi level for a broader range of dopings than found when $t' = 0$. Again, the dispersion along the k_x direction moves continuously across the Fermi level.

quasiparticle weight along the antinodal momentum direction, Z_{AN},[58] displayed in Fig. 13 as a function of temperature for different fillings. The quasiparticle fraction is consistently smaller for $t'/t = -0.1$ than for $t' = 0$ for all fillings. This can also be seen through the increase of the blue color in the dispersion curves in Fig. 11 when compared with Fig. 6.

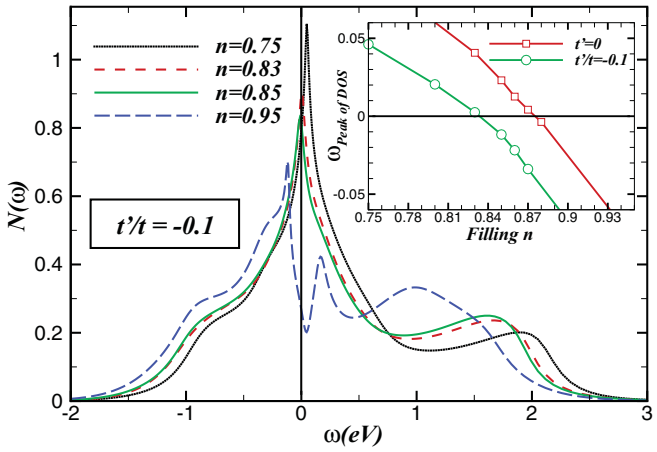

FIG. 12. (Color online) Single-particle density of states for $t'/t = -0.1$ when $U = 6t$, $N_c = 16, 4t = 1$, and $\beta = 48$. Inset: Comparison of the filling dependence of the position of the peak of the density of states (ω_p) for $t' = 0$ and $t'/t = -0.1$. As the filling changes, ω_p for $t' = 0$ crosses the Fermi level more quickly than for $t'/t = -0.1$.

D. Transport properties

Matrix element effects[75,76] and the low precision of inverse photoemission can complicate the direct measurement of the flat dispersion resulting in the van Hove singularity, making indirect probes like the Fermi surface topology[74,77] and

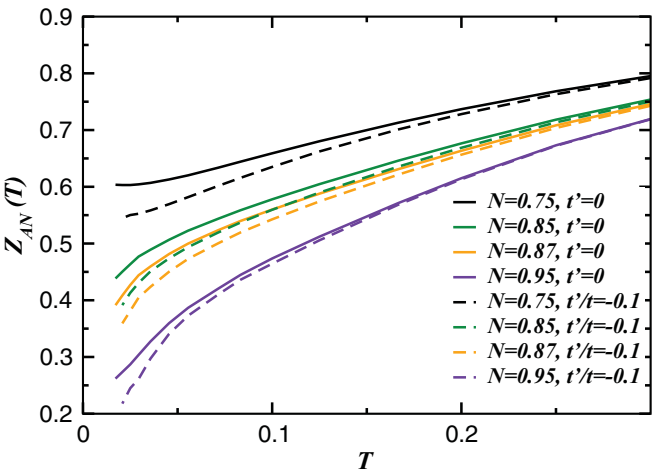

FIG. 13. (Color online) Temperature dependence of the Matsubara fraction along the antinodal direction, Z_{AN}, for various fillings for $t' = 0$ and $t'/t = -0.1$. At the same filling and temperature, the Matsubara fraction decreases when $t' < 0$.

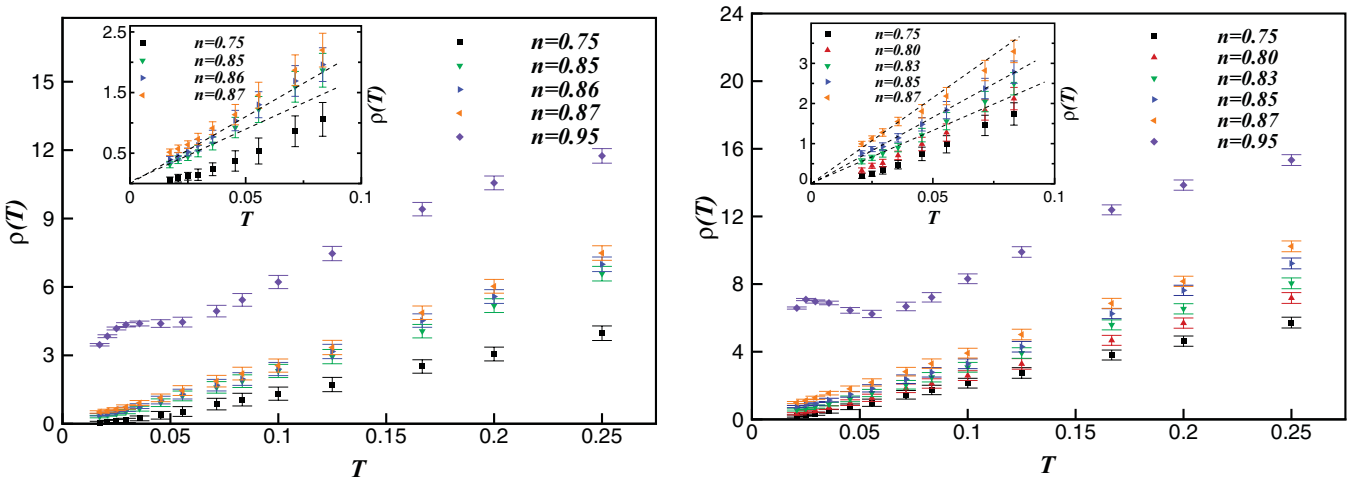

FIG. 14. (Color online) Resistivity vs temperature for $t' = 0$ (left) and $t'/t = -0.1$ (right) with $U = 6t$, $N_c = 16$, and $4t = 1$. The dashed lines in the insets are linear fits. For $t' = 0$, the resistivity shows linear-T behavior for $n = 0.85$ and 0.86. For $t'/t = -0.1$, the resistivity shows linear-T behavior from $n = 0.83$ to 0.87.

transport measurements more important. The van Hove singularity and the quantum critical point will also impact the transport properties of the system. Using the Kubo formula under the relaxation-time approximation in Eqs. (10) and (11), we obtain the resistivity, thermal conductivity, and thermopower in the Fermi liquid, marginal Fermi liquid, and pseudogap regions.

Figure 14 shows the resistivity as a function of temperature for $t' = 0$, left panel, and $t'/t = -0.1$, right panel. Linear resistivity reveals evidence of the marginal Fermi liquid because the electronic cross section is proportional to $-\Sigma''(\boldsymbol{k}_F, \omega = 0)$ at low T, and, as seen in Figs. 4 and 10, this self-energy is linear in T. Again, for $t' = 0$, a narrow range of fillings, from $n = 0.85$ to 0.86, displays a linear-T resistivity at low T, while for $t'/t = -0.1$, a larger range of filling, $n = 0.83$ to 0.87, exhibits a linear temperature dependence. The linear resistivity in the marginal Fermi liquid region is consistent with experiments.[44–47] For $n = 0.75$, both $t' = 0$ and $t'/t = -0.1$ show Fermi liquid character, with a resistivity that goes to zero quadratically when T approaches zero. The fact that the doping region with marginal Fermi liquid character increases with negative t' has consequences for the phase diagram near the quantum critical point, which we will discuss in Sec. IV.

According to the Wiedemann-Franz law, $\kappa/(\sigma T) = \pi^2/3$ ($k_B = e = 1$), the thermal conductivity of a Fermi liquid is inversely proportional to T.[57] Figure 15 shows that $\kappa \propto 1/T$ for $n = 0.75$ when $t'/t = 0$ and -0.1, but depends weakly on T for the marginal Fermi liquid and the pseudogap regions. The inset shows that, for $n = 0.75$, the Wiedemann-Franz ratio $\kappa/(\sigma T)$ approaches a constant that is less than $\pi^2/3$ when $T \leqslant 0.08$. Dahm *et al.*[78] investigated the two-dimensional Hubbard model for $n \simeq 0.9$ and also found a smaller Wiedemann-Franz ratio. However, we find that the Wiedemann-Franz ratio is larger than $\pi^2/3$ for the marginal Fermi liquid ($n = 0.85$) and pseudogap ($n = 0.95$) regions. We also see that the thermal conductivity becomes very small as $T \to 0$ for $n = 0.95$ and saturates to a constant for $n = 0.85$. So, when studying κ, the marginal Fermi liquid seems to separate the Fermi liquid from the pseudogap region. The dashed curves in Fig. 15 for $t'/t = -0.1$ data are always below the solid curves for $t' = 0$ when plotting κ. However, the $t'/t = -0.1$ data are above the $t' = 0$ results when we focus on the ratio $\kappa/\sigma T$. This implies that negative t' reduces the electrical conductivity more than the thermal conductivity.

Chakraborty *et al.*[53] argue that the thermopower changes sign near the quantum critical point, and that this is related to the development of a state with particle-hole symmetry. Figure 16 shows the thermopower S as a function of filling. For $t' = 0$ and $\beta = 58$, the filling at which S changes sign is roughly 0.80. We expect that the zero crossing of the thermopower will approach the critical filling of 0.85 for decreasing T. However, this is different from the filling, $n = 0.88$, at which the density of states displays particle-hole symmetry.

We find that due to the $\boldsymbol{k}$ dependence of the relaxation time and the electron group velocity, the filling at which the thermopower crosses zero does not occur at the filling where the density of states shows a particle-hole symmetry

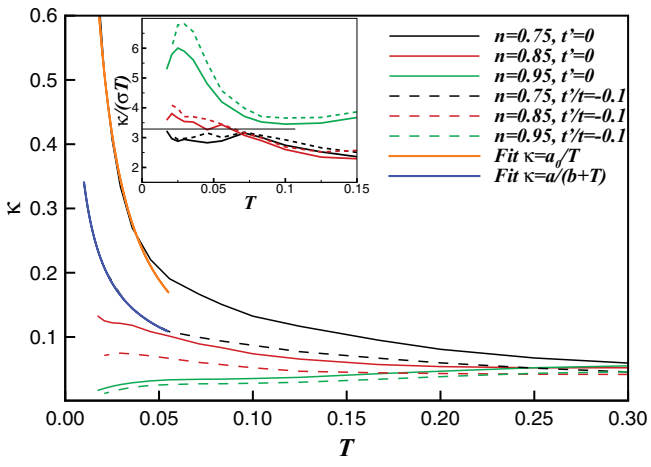

FIG. 15. (Color online) Thermal conductivity vs temperature for $U = 6t$, $N_c = 16$, and $4t = 1$. Inset: Wiedemann-Franz ratio for the same physical parameters. The horizontal solid line labels the constant $\pi^2/3$.

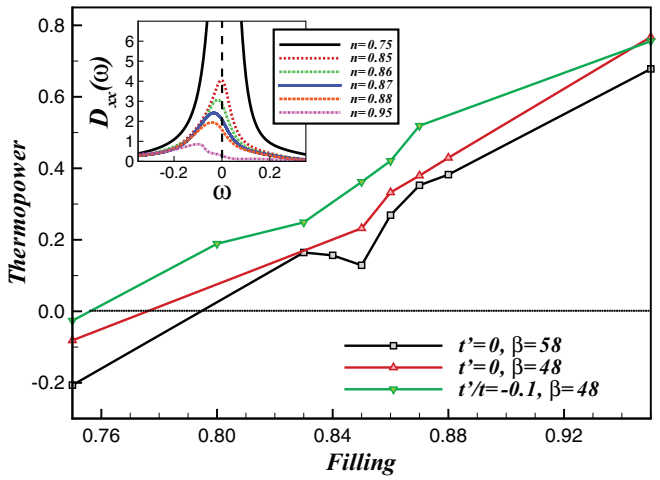

FIG. 16. (Color online) Thermopower as a function of filling for $U = 6t$, $N_c = 16$, and $4t = 1$. Lines are guides to the eyes. Inset: Frequency dependence of $\mathcal{D}_{xx}(\omega)$ [cf. Eq. (11) for different fillings when $t' = 0$, $\beta = 58$]. The slope of $\log \mathcal{D}_{xx}(\omega)$ at $\omega = 0$ is proportional to the thermopower according to Eq. (12).

at low energies. In Fermi liquid theory,[70] if we assume constant relaxation time and group velocity, the thermopower is proportional to the derivative of the logarithm of the density of states at the Fermi level. This would suggest a thermopower that changes sign as the van Hove singularity crosses the Fermi level. However, in this approach, $A(\boldsymbol{k},\omega)^2$ in Eq. (11) is approximated by $\delta(\omega - \epsilon_{\boldsymbol{k}})\tau$, where $\tau = \tau_{\boldsymbol{k}}$ is a $\boldsymbol{k}$-independent relaxation time. In addition, the electron group velocity we use in our calculation also has a $\boldsymbol{k}$ dependence:

$$v^x(\boldsymbol{k}) = \frac{\partial \epsilon^0_{\boldsymbol{k}}}{\partial \boldsymbol{k}_x} = 2t \sin k_x + 4t' \sin k_x \cos k_y. \qquad (14)$$

If we compare the quantity $\mathcal{D}_{xx}(\omega)$ (the inset of Fig. 16) and the density of states (Fig. 5) for different fillings and the same $t' = 0$, we find that the effect of $v^x(\boldsymbol{k})^2$ is to pull the peak of the density of states to the left, because the $\sin k_x$ term suppresses the contribution of the van Hove singularity at $X(\pi,0)$ and enhances the contribution from the states below the Fermi level. As a result, the thermopower changes sign continuously and at a filling where the quantity $\mathcal{D}(\omega)$ has a zero slope at the Fermi level, around $n = 0.85$. As noted by Chakraborty *et al.*,[53] this filling is different from the one where the density of states displays particle-hole symmetry, $n = 0.88$ for $t' = 0$. The impact of the van Hove singularity on the thermopower and other transport coefficients is diminished by the fact that the van Hove singularity comes predominantly from a region in $\boldsymbol{k}$ space where the group velocity goes through zero.

IV. DISCUSSION

The results presented here have implications for both the quantum critical phase diagram and the proximity of the superconducting dome to the quantum critical point.

The close proximity of the quantum critical filling and the filling where the van Hove singularity crosses the Fermi level suggests that the two are related or even concomitant. Near the quantum critical point, we find that the flat part of the dispersion orthogonal to the antinodal direction is pinned to the Fermi level, but not the dispersion along that direction (Fig. 6). We also find that the low-energy density of states exhibits particle-hole symmetry (Fig. 5). The linear-T resistivity and self-energy, characteristic of a marginal Fermi liquid, are observed for the same fillings where this pinning is observed. Within the dynamical mean-field approximation (DMFA),[16] it is known that if the van Hove singularity is pinned to the Fermi level for the noninteracting case, it remains pinned even for the interacting case due to the momentum-independent nature of the self-energy. In addition, a van Hove singularity initially away from the Fermi level will tend to move toward the Fermi level due to the narrowing of the coherent component of the band resulting from electronic correlations. In the simplest Fermi liquid picture, the coherent part of the single-particle Green function $G(\boldsymbol{k},\omega) = Z(\boldsymbol{k})/[\omega + i0^+ - Z(\boldsymbol{k})\epsilon(\boldsymbol{k})]$. So, if $Z(\boldsymbol{k})$ becomes small for some values of $\boldsymbol{k}$, then we would expect to see a flattening of the observed quasiparticle dispersion, $Z(\boldsymbol{k})\epsilon(\boldsymbol{k})$, accompanied by a shift of the peak toward the Fermi level with a vanishing weight. The new result of our work is that the nonlocal correlations included in the DCA, but absent in the DMFA, are able to move the van Hove singularity, with finite weight, to and even across the Fermi level. This cannot be due solely to the narrowing of the coherent part of the band, since the van Hove singularity crosses the Fermi level where the quasiparticle fraction Z is already zero.

In addition, a noninteracting picture of the van Hove singularity cannot completely describe the superconducting transition in the vicinity of the critical filling. In a BCS superconductor, the transition is driven by a logarithmic divergence of the bare pairing bubble as the temperature falls. In a recent work,[59] the bare d-wave pairing susceptibility χ'_{0d} of the 2D Hubbard model was found to diverge algebraically as $\frac{1}{\sqrt{T}}$ at the quantum critical filling, instead of logarithmically, giving rise to a higher T_c. In the simulation, we traced the origin of this algebraic behavior to a component of the dynamic bare bubble, which scaled as $\chi''_{0d}(\omega)/\omega = T^{-3/2}H(\omega/T)$ (see Fig. 1). A van Hove singularity is known to enhance the divergence of the bare pairing bubble. Since the bare d-wave pairing susceptibility is dressed only by the self-energy, with no vertex corrections, a van Hove singularity seems to be the most likely explanation of its enhanced divergence. However, we found that a simple noninteracting picture with a van Hove singularity at the Fermi level does not completely explain the observed phenomena. The standard quadratic dispersion gives a logarithmic divergence of χ'_{0d} for the half-filled model. A hypothetical quartic dispersion yields the observed algebraic divergence for χ'_{0d}, but does not give the correct scaling for the imaginary part of the bare susceptibility found in Yang *et al.*[59] The latter is a consequence of the proximity to a quantum critical point, but not necessarily part of the van Hove scenario.

Our results also shed additional light on the quantum critical phase diagram. We found previously[79,80] that when $t' > 0$, there is a first-order phase separation transition with a first-order line of coexistence in the μ-T phase diagram, as shown in Fig. 17. In analogy with liquid-gas mixtures, we identify the two phases as a Mott liquid, which is insulating and incompressible with well-formed local moments and short-ranged order, and a Mott gas, which is a weakly compressible

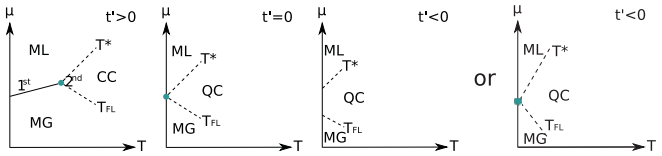

FIG. 17. (Color online) Schematic chemical potential-temperature (μ-T) phase diagram for three values of t': (from left to right) $t' > 0$, $t' = 0$, $t' < 0$ scenario presented in this paper and a $t' < 0$ scenario based on a Lifshitz transition. CC (QC) indicates the classical (quantum) critical region. ML (MG) indicates the Mott liquid (gas) region. T^* is the crossover temperature between the Mott liquid and the critical region, $T_{\rm FL}$ separates the Mott gas from the critical region. Note that here we have ignored other phases to focus attention on the quantum critical region.

metallic Fermi liquid. The two phases have the same symmetry, so the first-order line of coexistence terminates at a second-order point where the charge susceptibility diverges. In analogy to other liquid-gas mixtures, there is a fan-shaped region dominated by fluctuations for temperatures above the critical point with neither liquid nor gas character. When $t' \to 0$, the critical point goes continuously to zero temperature and thus becomes a quantum critical point.[80] Above the quantum critical point, the marginal Fermi liquid region is found to exist in the V-shaped quantum critical region. Inside this region, the only scale is the temperature [like Eqs. (8) and (9)]. T^* is the temperature separating the marginal Fermi liquid from the pseudogap region. T^* does not separate the quantum critical region from a region of hidden order. Rather, in our scenario, it is only the boundary of the quantum critical region. As we cross from the quantum critical region to the Mott liquid, the character of the Mott liquid becomes apparent, including a pseudogap.

Here we consider the effect of a negative next-near-neighbor hopping t' on the single-particle dispersion. We find that for $t'/t = -0.1$, the flat part of the dispersion orthogonal to the antinode remains in close proximity to the Fermi level for a larger range of fillings ($0.83 \leqslant n \leqslant 0.87$) when compared with the $t' = 0$ result. We find that the resistivity displays a linear-T dependence, and the self-energy displays MFL characteristics in the same range of doping. We also note that the single-particle spectrum is less coherent in the center of this doping region than it is at the quantum critical filling when $t' = 0$. These observations are consistent with an increase in the doping region of marginal Fermi liquid character when $t'/t < 0$.

There are several different scenarios that may explain this behavior. Since the doping region where the van Hove singularity is near the Fermi level increases with decreasing t'/t, perhaps the simplest understanding of this behavior is that the van Hove singularity *pinning* gives rise to the marginal Fermi liquid behavior.[12–14] Another possibility is that both T and negative t' are relevant variables, or variables that, when finite, move the system away from a critical point. In addition, they are roughly similar in their effect, in that when $t' = T = 0$, the doping region of marginal Fermi liquid character shrinks to a point, but the region increases with either increasing T or decreasing t'. Thus when $t' < 0$, the quantum critical point may be viewed as moving to negative temperatures so that the quantum critical region broadens to allow the linear-T resistivity and the pinning of the flat k_y dispersion to the Fermi level to exist for a wider range of fillings (compare, e.g., the third panel of Fig. 17 and the inset of Fig. 1). However, this interpretation is not consistent with scaling theory, where we expect a finite low-temperature scale like T_F or T^* to emerge for any set of parameters that take us away from the quantum critical point. Another possibility is that the change in Fermi surface topology associated with the van Hove singularity crossing the Fermi level can introduce *Lifshitz* singularities in the free energy.[81–87] This scenario will mean a line of zero-temperature critical points in the t'-μ plane beyond the quantum critical point as the control parameter t' is decreased from zero to negative values in the t'-μ plane. For positive t', the Lifshitz transition may yield a line of first-order critical points in t'-μ plane that terminates at the quantum critical point for $t' = 0$. To understand our results, the line of Lifshitz transitions for negative values of t'/t must yield an associated V-shaped region of quantum criticality that becomes flatter as t' decreases, as shown on the right in Fig. 17. Finally, another mechanism enhanced by the van Hove singularity is the *Pomeranchuk instability*[88,89] of the Fermi surface, where the Fermi surface is distorted to break the C_4 symmetry of the square lattice. The possibility of Lifshitz and Pomeranchuk transitions is being studied currently and will be published elsewhere.

There is some experimental evidence[74] in the cuprates that there is a change in Fermi surface topology and an associated Fermi level crossing of the van Hove singularity at a doping that is larger than the doping at which T_c is maximum, while still being within the dome. On the other hand, we find that the van Hove singularity crosses the Fermi level at a slightly smaller doping than the optimal doping. This disagreement can be due to the other effects present in the real systems, e.g., phonons that are not incorporated in this model calculation, or the strong doping dependence of the strength of the pairing interaction[59] seen in the simulations.

The transport provides some additional evidence for the van Hove singularity. In our calculations, the low-energy particle-hole symmetry and the change in sign of the thermopower with doping near the critical value are both due to the crossing of the van Hove singularity. However, the doping associated with the van Hove crossing differs from that where the thermopower is zero due to the anisotropy of the group velocity on the Fermi surface.

V. CONCLUSION

We explore the role of the van Hove singularity in the quantum criticality observed at finite doping in the Hubbard model.[58] Near the quantum critical filling, we find a van Hove singularity due to a flattening of the dispersion near the Fermi level. The motion of the flat part of the dispersion along the antinodal direction is anisotropic. The part along the antinode moves continuously through the Fermi level. The part orthogonal to this direction is pinned near the Fermi level at a filling where the self-energy, transport, and energies[73] also display marginal Fermi liquid behavior, and the quasiparticle fraction vanishes.[58] Many authors have proposed that the van Hove singularity near the Fermi level

will enhance superconductivity by enhancing the divergence of the bare pairing bubble. Indeed, we found previously that the superconducting dome surrounds the critical doping where the real part of the pairing bubble diverges algebraically, replacing the Fermi liquid log divergence.[59] However, a simple noninteracting picture with the van Hove singularity at the Fermi level does not explain the quantum critical scaling of the bare dynamic pairing susceptibility. We also found previously that a positive t' is the control parameter for a first-order phase separation transition which is terminated by a second-order critical point. As $t' \to 0$, this second-order terminus is driven to zero temperature, yielding the quantum critical point.[80] Here we explore the effect of a negative t', and we find that it is a relevant variable that increases the extent in doping (and chemical potential) of the quantum critical region characterized by marginal Fermi liquid behavior.

ACKNOWLEDGMENTS

We would like to thank Piers Coleman, Jan Zaanen, Thomas Pruschke, H. R. Krishnamurthy, Sebastian Schmitt, George Kastrinakis, Ka-Ming Tam, Matthias Vojta, Masa Imada, Walter Metzner, and Jian-Huang She for useful conversations. We also thank Robert Markiewicz for a careful reading of the manuscript and for providing insightful suggestions. This work is supported by DOE SciDAC DE-FC02-06ER25792 (S.P., S.X.Y., K.M., M.J.), and NSF Grants No. OISE-0952300 (K.S.C., S.X.Y., S.Q.S., J.M.) and No. DMR-0706379 (D.G. and M.J.). Supercomputer support was provided by the NSF TeraGrid under Grant No. TG-DMR100007. This research also used resources of the National Center for Computational Sciences at Oak Ridge National Laboratory, which is supported by the Office of Science of the US Department of Energy under Contract No. DE-AC05-00OR22725.

[1] J. Labbè and J. Bok, Europhys. Lett. **3**, 1225 (1987).
[2] J. Friedel, J. Phys. (Paris) **48**, 1787 (1987).
[3] D. M. Newns, H. R. Krishnamurthy, P. C. Pattnaik, C. C. Tsuei, and C. L. Kane, Phys. Rev. Lett. **69**, 1264 (1992).
[4] R. S. Markiewicz, J. Phys. Chem. Solids **58**, 1179 (1997).
[5] D. S. Dessau *et al.*, Phys. Rev. Lett. **71**, 2781 (1993).
[6] K. Gofron, J. C. Campuzano, A. A. Abrikosov, M. Lindroos, A. Bansil, H. Ding, D. Koelling, and B. Dabrowski, Phys. Rev. Lett. **73**, 3302 (1994).
[7] A. Abrikosov, J. Campuzano, and K. Gofron, Physica C **214**, 73 (1993).
[8] J. C. Campuzano, K. Gofron, H. Ding, R. Liu, B. Dabrowski, and B. J. W. Veal, J. Low Temp. Phys. **95**, 245 (1994).
[9] D. M. King, Z. X. Shen, D. S. Dessau, D. S. Marshall, C. H. Park, W. E. Spicer, J. L. Peng, Z. Y. Li, and R. L. Greene, Phys. Rev. Lett. **73**, 3298 (1994).
[10] A. Piriou, N. Jenkins, C. Berthod, I. Maggio-Aprile, and O. Fischer, Nat. Commun. **2**, 221 (2011).
[11] J. L. McChesney, A. Bostwick, T. Ohta, T. Seyller, K. Horn, J. González, and E. Rotenberg, Phys. Rev. Lett. **104**, 136803 (2010).
[12] P. C. Pattnaik, C. L. Kane, D. M. Newns, and C. C. Tsuei, Phys. Rev. B **45**, 5714 (1992).
[13] D. M. Newns, C. C. Tsuei, R. P. Huebener, P. J. M. van Bentum, P. C. Pattnaik, and C. C. Chi, Phys. Rev. Lett. **73**, 1695 (1994).
[14] C. C. Tsuei, D. M. Newns, C. C. Chi, and P. C. Pattnaik, Phys. Rev. Lett. **65**, 2724 (1990).
[15] C. M. Varma, P. B. Littlewood, S. Schmitt-Rink, E. Abrahams, and A. E. Ruckenstein, Phys. Rev. Lett. **63**, 1996 (1989).
[16] P. Majumdar and H. R. Krishnamurthy, e-print arXiv:cond–mat/9604057.
[17] F. Assaad and M. Imada, Eur. Phys. J. B **10**, 595 (1999).
[18] M. Imada, A. Fujimori, and Y. Tokura, Rev. Mod. Phys. **70**, 1039 (1998).
[19] E. Dagotto, A. Nazarenko, and M. Boninsegni, Phys. Rev. Lett. **73**, 728 (1994).
[20] D. M. Newns, P. C. Pattnaik, and C. C. Tsuei, Phys. Rev. B **43**, 3075 (1991).
[21] S. Gopalan, O. Gunnarsson, and O. K. Andersen, Phys. Rev. B **46**, 11798 (1992).
[22] R. J. Radtke and M. R. Norman, Phys. Rev. B **50**, 9554 (1994).
[23] R. Hlubina and T. M. Rice, Phys. Rev. B **51**, 9253 (1995).
[24] D. M. Newns, C. C. Tsuei, and P. C. Pattnaik, Phys. Rev. B **52**, 13611 (1995).
[25] I. Dzyaloshinskii, J. Phys. I **6**, 119 (1996).
[26] D. Djajaputra and J. Ruvalds, e-print arXiv:cond-mat/9604057.
[27] R. G. Dias, J. Phys. Condens. Matter **12**, 9053 (2000).
[28] C. J. Halboth and W. Metzner, Phys. Rev. B **61**, 7364 (2000).
[29] G. Kastrinakis, Physica C **340**, 119 (2000).
[30] V. Y. Irkhin and A. A. Katanin, Phys. Rev. B **64**, 205105 (2001).
[31] V. Y. Irkhin, A. A. Katanin, and M. I. Katsnelson, Phys. Rev. Lett. **89**, 076401 (2002).
[32] K. G. Sandeman, G. G. Lonzarich, and A. J. Schofield, Phys. Rev. Lett. **90**, 167005 (2003).
[33] A. A. Katanin and A. P. Kampf, Phys. Rev. Lett. **93**, 106406 (2004).
[34] R. S. Markiewicz, Phys. Rev. B **70**, 174518 (2004).
[35] G. Kastrinakis, Phys. Rev. B **71**, 014520 (2005).
[36] K. M. Shen, N. Kikugawa, C. Bergemann, L. Balicas, F. Baumberger, W. Meevasana, N. J. C. Ingle, Y. Maeno, Z.-X. Shen, and A. P. Mackenzie, Phys. Rev. Lett. **99**, 187001 (2007).
[37] T. Shibauchi, L. Krusin-Elbaum, M. Hasegawa, Y. Kasahara, R. Okazaki, and Y. Matsuda, Proc. Natl. Acad. Sci. USA **105**, 7120 (2008).
[38] A. Tamai *et al.*, Phys. Rev. Lett. **101**, 026407 (2008).
[39] R. Zitko, J. Bonca, and T. Pruschke, Phys. Rev. B **80**, 245112 (2009).
[40] A. Katanin, Phys. Rev. B **81**, 165118 (2010).
[41] S. Schmitt, Phys. Rev. B **82**, 155126 (2010).
[42] S. E. Sebastian, N. Harrison, M. M. Altarawneh, C. H. Mielke, R. Liang, D. A. Bonn, W. N. Hardy, and G. G. Lonzarich, Proc. Natl. Acad. Sci. USA **107**, 6175 (2010).
[43] L. Taillefer, Annu. Rev. Condens. Matter Phys. **1**, 51 (2010).
[44] Y. Ando, S. Komiya, K. Segawa, S. Ono, and Y. Kurita, Phys. Rev. Lett. **93**, 267001 (2004).
[45] R. Daou *et al.*, Nat. Phys. **5**, 31 (2009).
[46] R. A. Cooper *et al.*, Science **323**, 603 (2009).
[47] M. Gurvitch and A. T. Fiory, Phys. Rev. Lett. **59**, 1337 (1987).

[48]B. Wuyts, V. V. Moshchalkov, and Y. Bruynseraede, Phys. Rev. B **53**, 9418 (1996).
[49]C. Uher, A. B. Kaiser, E. Gmelin, and L. Walz, Phys. Rev. B **36**, 5676 (1987).
[50]A. J. Schofield, Contemp. Phys. **40**, 95 (1999).
[51]X. F. Sun, S. Komiya, and Y. Ando, Phys. Rev. B **67**, 184512 (2003).
[52]R. K. Williams, J. O. Scarbrough, J. M. Schmitz, and J. R. Thompson, Phys. Rev. B **57**, 10923 (1998).
[53]S. Chakraborty, D. Galanakis, and P. Phillips, Phys. Rev. B **82**, 214503 (2010).
[54]H. J. Trodahl, Phys. Rev. B **51**, 6175 (1995).
[55]M. Gurvitch, J. M. Valles, A. M. Cucolo, R. C. Dynes, J. P. Garno, L. F. Schneemeyer, and J. V. Waszczak, Phys. Rev. Lett. **63**, 1008 (1989).
[56]F. Steglich, *High Temperature Superconductors and Materials and Mechanisms of Superconductivity* (North Holland, Amsterdam, 1988), p. 1010.
[57]G. Wiedemann and R. Franz, Ann. Phys. **165**, 497 (1853).
[58]N. S. Vidhyadhiraja, A. Macridin, C. Sen, M. Jarrell, and M. Ma, Phys. Rev. Lett. **102**, 206407 (2009).
[59]S.-X. Yang, H. Fotso, S.-Q. Su, D. Galanakis, E. Khatami, J.-H. She, J. Moreno, J. Zaanen, and M. Jarrell, Phys. Rev. Lett. **106**, 047004 (2011).
[60]M. Jarrell and J. E. Gubernatis, Phys. Rep. **269**, 133 (1996).
[61]X. Wang, E. Gull, L. de' Medici, M. Capone, and A. J. Millis, Phys. Rev. B **80**, 045101 (2009).
[62]M. H. Hettler, A. N. Tahvildar-Zadeh, M. Jarrell, T. Pruschke, and H. R. Krishnamurthy, Phys. Rev. B **58**, R7475 (1998).
[63]M. H. Hettler, M. Mukherjee, M. Jarrell, and H. R. Krishnamurthy, Phys. Rev. B **61**, 12739 (2000).
[64]A. N. Rubtsov, V. V. Savkin, and A. I. Lichtenstein, Phys. Rev. B **72**, 035122 (2005).
[65]N. Blümer, Phys. Rev. B **76**, 205120 (2007).
[66]J. E. Hirsch and R. M. Fye, Phys. Rev. Lett. **56**, 2521 (1986).
[67]M. Jarrell, T. Maier, C. Huscroft, and S. Moukouri, Phys. Rev. B **64**, 195130 (2001).
[68]C. M. Varma, Z. Nussinov, and W. van Saarloos, Phys. Rep. **361**, 267 (2002).
[69]R. Kubo, *Lectures in Theoretical Physics* (Interscience, New York, 1959), Vol. 1, p. 120.
[70]J. A. Stovneng and P. Lipavský, Phys. Rev. B **42**, 9214 (1990).
[71]A. C. Hewson, *The Kondo Problem to Heavy Fermions* (Cambridge University Press, Cambridge, 1993).
[72]R. S. Markiewicz, S. Sahrakorpi, and A. Bansil, Phys. Rev. B **76**, 174514 (2007).
[73]K. Mikelsons, E. Khatami, D. Galanakis, A. Macridin, J. Moreno, and M. Jarrell, Phys. Rev. B **80**, 140505 (2009).
[74]A. Kaminski, S. Rosenkranz, H. M. Fretwell, M. R. Norman, M. Randeria, J. C. Campuzano, J.-M. Park, Z. Z. Li, and H. Raffy, Phys. Rev. B **73**, 174511 (2006).
[75]A. Bansil and M. Lindroos, J. Phys. Chem. Solids **59**, 1879 (1998).
[76]A. Bansil and M. Lindroos, Phys. Rev. Lett. **83**, 5154 (1999).
[77]T. Yoshida *et al.*, Phys. Rev. B **63**, 220501 (2001).
[78]T. Dahm, L. Tewordt, and S. Wermbter, Phys. Rev. B **49**, 748 (1994).
[79]A. Macridin, M. Jarrell, and T. Maier, Phys. Rev. B **74**, 085104 (2006).
[80]E. Khatami, K. Mikelsons, D. Galanakis, A. Macridin, J. Moreno, R. T. Scalettar, and M. Jarrell, Phys. Rev. B **81**, 201101 (2010).
[81]Y. Yamaji, T. Misawa, and M. Imada, J. Phys. Soc. Jpn. **75**, 094719 (2006).
[82]M. R. Norman, J. Lin, and A. J. Millis, Phys. Rev. B **81**, 180513 (2010).
[83]M. Imada, Phys. Rev. B **72**, 075113 (2005).
[84]T. Misawa, Y. Yamaji, and M. Imada, J. Phys. Soc. Jpn. **75**, 083705 (2006).
[85]T. Misawa and M. Imada, Phys. Rev. B **75**, 115121 (2007).
[86]Y. Yamaji, T. Misawa, and M. Imada, J. Phys. Soc. Jpn. **76**, 063702 (2007).
[87]M. Imada, T. Misawa, and Y. Yamaji, J. Phys. Condens. Matter **22**, 164206 (2010).
[88]C. J. Halboth and W. Metzner, Phys. Rev. Lett. **85**, 5162 (2000).
[89]H. Yamase, V. Oganesyan, and W. Metzner, Phys. Rev. B **72**, 035114 (2005).